A grapefruit microstructure fiber temperature sensor coated with liquid crystal based on waist-enlarged taper*

WANG Feng[1], LI Jiaxuan[2], ZHANG Rongjing[2], and FU Xinghu[2]**

1. College of Mechanical and Electrical Engineering, Hebei Normal University of Science & Technology, Qinhuangdao 066004, China

2. School of Information Science and Engineering, Key Laboratory for Special Fiber and Fiber Sensor of Hebei Province, Yanshan University, Qinhuangdao 066004, China

(Received 7 January 2023; Revised 8 September 2023)

In this paper, a grapefruit microstructure fiber (GMF) temperature sensor coated with liquid crystal (LC) based on waist-enlarged taper is proposed and fabricated, and its temperature sensing characteristics are analyzed. The waist-enlarged taper is formed at the fusion point between single mode fiber (SMF) and GMF. The capillary glass tube is sleeved outside GMF, LC is filled into the capillary glass tube, and its two ends are finally sealed to form a sensor. The experimental results show that when the length of GMF is 2.5 cm, the temperature sensitivity of the sensor can reach up to 195.3 pm/°C in the range of 30—90 °C, and it has a good stability for reuse. Thereby, it can be used in biochemical, industrial production and other temperature detection areas.

Document code: A **Article ID:** 1673-1905(2024)03-0142-5
DOI https://doi.org/10.1007/s11801-024-3003-y

Compared with traditional temperature sensors, optical fiber temperature sensors have many advantages, such as small size[1], strong electromagnetic interference resistance[2], high sensitivity[3], etc. In recent years, microstructure fibers have been used in high temperature[4], humidity[5] and torsion measurement[6]. Domestic and foreign scholars change the transmission mechanism of microstructure fibers by filling sensitive materials, and realize temperature sensors by combining the characteristics of liquid crystal (LC)[7] that is sensitive to temperature environments. For example, HUANG et al[8] proposed an LC filled side hole fiber temperature sensor, which has a temperature sensitivity of −1.36 nm/°C in the range of 22—27 °C. HU et al[9] proposed a fiber tip temperature sensor based on cholesteric LC. The temperature sensitivity is 9.167 nm/°C in 23—29 °C. LIN et al[10] proposed an LC filled hollow core fiber temperature sensor. The temperature sensitivity can reach −1.041 nm/°C in 20—30 °C. It can be seen from the above that when the external temperature changes, the refractive index of LC will also change accordingly, and the temperature detection can be realized. Therefore, this paper proposes a grapefruit microstructure fiber (GMF) temperature sensor coated with LC based on waist-enlarged taper, and analyzes its temperature sensing characteristics. During the preparation of the sensor, the waist-enlarged taper is formed between the fusion point of single mode fiber (SMF) and GMF. Then we sleeve the capillary glass tube outside the GMF, and fill the LC into the capillary glass tube, and finally seal its two ends with AB glue. The SMF has a core diameter of 9 μm and a cladding diameter of 125 μm. There are six grapefruit air holes near the core in the GMF. The proposed GMF sensor is shown in Fig.1. The parameters of GMF are shown in Tab.1.

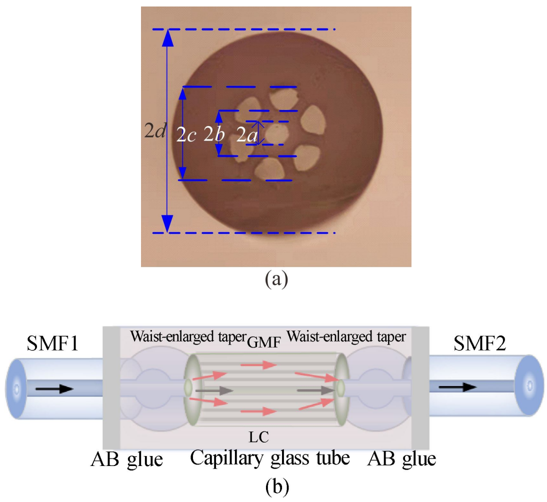

Fig.1 (a) Cross section of GMF; (b) Structure of the proposed GMF sensor

* This work has been supported by the Science and Technology Project of Hebei Education Department (No.ZD2022108), the Natural Science Foundation of Hebei Province (No.F2021203102), and the Post-graduate's Innovation Fund Project of Hebei Province (No.CXZZSS2022118).
** E-mail: fuxinghu@ysu.edu.cn

Tab.1 Structural parameters of GMF

Structure	Radius (μm)	Refractive index
Core (*a*)	10.0	1.473
Inner cladding (*b*)	18.0	1.457
Air hole (*c*)	34.5	1.000
Outer cladding (*d*)	62.5	1.457

In Fig.1(b), the laser emitted by the light source passes through the SMF and is transmitted forward in its core in the basic mode. When the laser is transmitted to the fusion point between SMF1 and GMF, it will be divided into two paths. One path of laser will enter the core of GMF and continue to transmit as the core mode. The other path of laser will enter the cladding of GMF and be transmitted forward as the cladding mode in the cladding of GMF. However, the refractive index of the core and cladding of GMF is different, so the laser in the core and cladding will have optical path difference. When the two beams are transmitted to the fusion point between GMF and SMF2, they will be coupled into SMF2, and the two beams will interfere to form a Mach-Zehnder interferometer. At this time, the interference light intensity[11] of the mode can be expressed as

$$I(\lambda)=I_1+I_2+2\sqrt{I_1I_2}\cos\varphi, \tag{1}$$

where I_1 and I_2 are the intensities of transmitted light in the core and cladding of GMF, respectively. φ is the phase difference formed by two beams, which can be expressed as

$$\varphi=\frac{2\pi\left(n_{\mathrm{eff}}^{\mathrm{r}}-n_{\mathrm{eff}}^{\mathrm{cl}}\right)L}{\lambda}=\frac{2\pi\Delta n_{\mathrm{eff}}L}{\lambda}, \tag{2}$$

where Δn_{eff} is the difference of effective refractive index between core mode and cladding mode of GMF. $n_{\mathrm{eff}}^{\mathrm{r}}$ and $n_{\mathrm{eff}}^{\mathrm{cl}}$ are the effective refractive indexes of the core mode and cladding mode. L is the length of GMF. λ is the wavelength of transmitted light in GMF. λ_m is the wavelength of the mth interference fringe, namely

$$\lambda_m=\frac{\Delta n_{\mathrm{eff}}L}{m}. \tag{3}$$

When the temperature rises, Δn_{eff} will change accordingly. The thermal optical coefficient has a great influence on the Δn_{eff}, which is 6.45×10^{-6}/°C. At the same time, GMF has thermal expansion effect, which will change the length of GMF. The thermal expansion coefficient is 5.5×10^{-7}/°C. Because the thermal expansion coefficient is far less than the thermal optical coefficient, the effect of the former on the transmission spectrum is very small, and the change of GMF length can be ignored here. The wavelength shift of the mth order interference fringe in spectrum can be expressed as

$$\Delta\lambda_m=\frac{(\Delta n_{\mathrm{eff}}+\Delta n)L}{m}-\frac{\Delta n_{\mathrm{eff}}L}{m}=\frac{\Delta nL}{m}, \tag{4}$$

where $\Delta\lambda_m$ is the wavelength shift of the transmission spectrum with temperature change. Δn is the change of Δn_{eff} with temperature change. When the temperature increases, the ordinary light refractive index of the LC increases continuously, and the Δn is positive, the spectrum will shift to the long wave direction, that is, red shift. Therefore, it is possible to detect the $\Delta\lambda_m$ to realize temperature detection.

The prepared sensor is used for temperature characteristic detection. The experimental device consists of broadband light source (ASE, wavelength range of 1 520—1 610 nm, output power of 50 mW), optical spectral analyzer (OSA, AQ6375) and temperature controller (WHL-30B, resolution of 0.1 °C). The experimental setup for temperature measurement is shown in Fig.2.

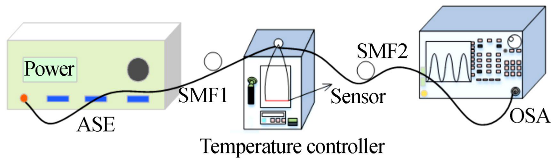

Fig.2 Experimental setup for temperature measurement

In experiment, the temperature range is set to 30—90 °C, and the transmission spectrum is recorded once every 10 °C rise. The GMF length is 2.5 cm, and the two ends of the GMF are connected with the SMF by secondary discharge to form a waist-enlarged taper, and its temperature sensing characteristics are analyzed. The transmission spectral shifts with the increase of temperature are shown in Fig.3.

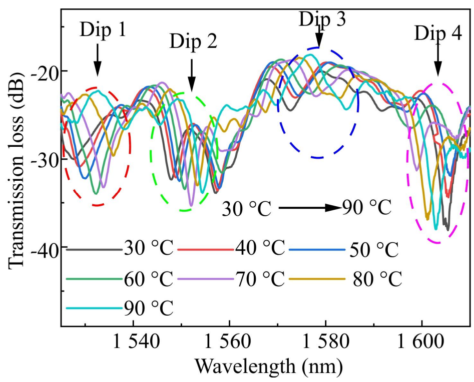

Fig.3 Transmission spectral shifts with the increase of temperature

It can be seen from Fig.3 that the transmission spectrum shifts to the long wave direction when the temperature rises from 30 °C to 90 °C. In order to analyze the relationship between wavelength shift and temperature, Dip 1, Dip 2, Dip 3 and Dip 4 are selected for analysis. The linear fitting results are shown in Fig.4.

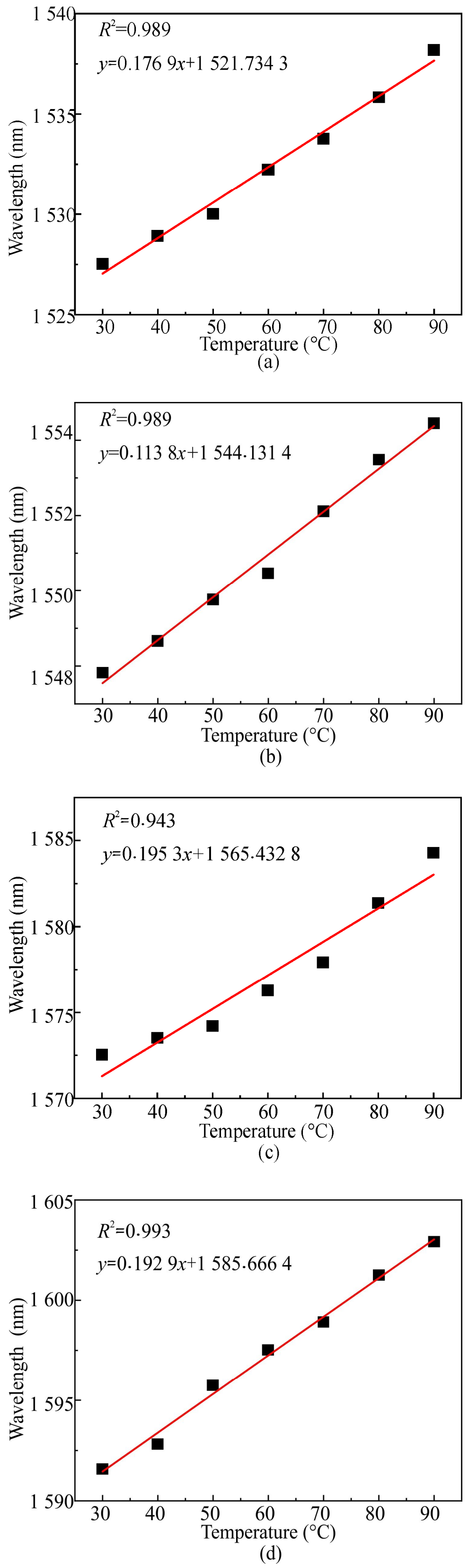

Fig.4 Linear fitting results: (a) Dip 1; (b) Dip 2; (c) Dip 3; (d) Dip 4

It can be seen from Fig.4 that in the temperature range of 30—90 °C, the shifts of Dip 1, Dip 2, Dip 3 and Dip 4 are 11.01 nm, 6.59 nm, 12.23 nm and 11.48 nm, respectively. So it can be calculated that the temperature sensitivity is 176.9 pm/°C, 113.8 pm/°C, 195.3 pm/°C and 192.9 pm/°C, respectively. Therefore, the temperature sensitivity of this sensor can reach up to 195.3 pm/°C. According to the temperature characteristic of LC, the refractive index of LC increases with the increasing temperature. At the same time, GMF has a thermo optical effect, which makes Δn a positive value. Therefore, when the temperature rises from 30 °C to 90 °C, the transmission spectrum moves to the long wave direction.

The finite element method is used to simulate the mode of GMF. The simulation results are shown in Fig.5 and the effective refractive index corresponding to each mode is shown in Tab.2.

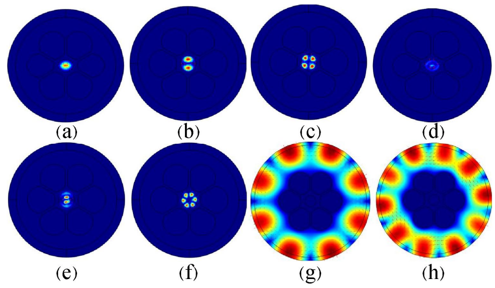

Fig.5 Simulation of transmission modes for GMF: (a) LP_{01}; (b) LP_{11}; (c) LP_{21}; (d) LP_{02}; (e) LP_{12}; (f) LP_{31}; (g) LP_{41}; (h) LP_{51}

Tab.2 Effective refractive index corresponding to each mode

Mode	Refractive index
LP_{01}	1.472 0
LP_{11}	1.470 6
LP_{21}	1.468 7
LP_{02}	1.468 0
LP_{12}	1.465 0
LP_{31}	1.462 3
LP_{41}	1.456 3
LP_{51}	1.456 0

The difference of effective refractive index between core mode and cladding mode of GMF can be obtained by

$$\Delta n_{\mathrm{eff}} = \frac{\xi \lambda_0^2}{L}, \tag{5}$$

where ξ is the peak x-coordinate in Fig.6, λ_0 is the wavelength of the incoming light and L is the length of the sensor. Based on the simulation results and Eq.(5), the transmission mode participating in the interference can be obtained. The fast Fourier transform (FFT) of transmission spectrum is shown in Fig.6, and it can be seen that there are five high-order mode transmissions.

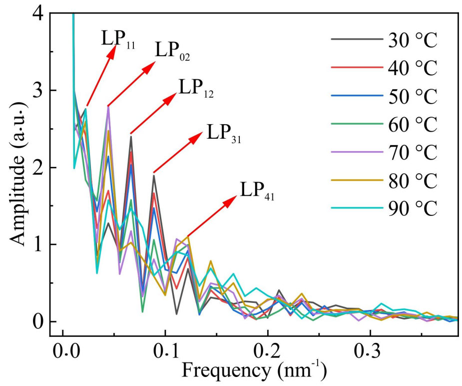

Fig.6 FFT of transmission spectra

In order to test the stability of the sensor, we repeated the experiment on the sensor one week later and compared it with the first experiment results, as shown in Fig.7.

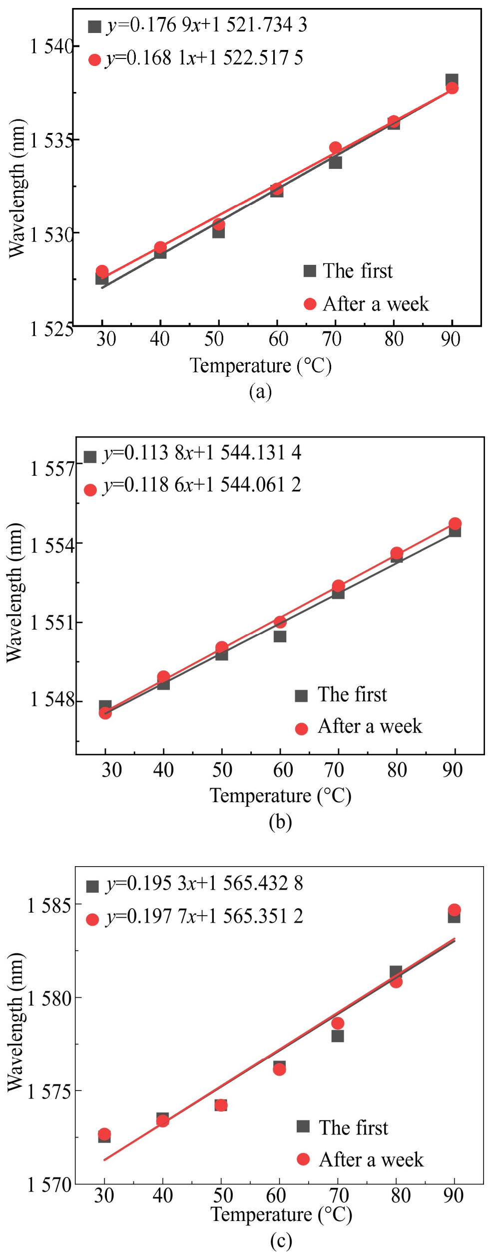

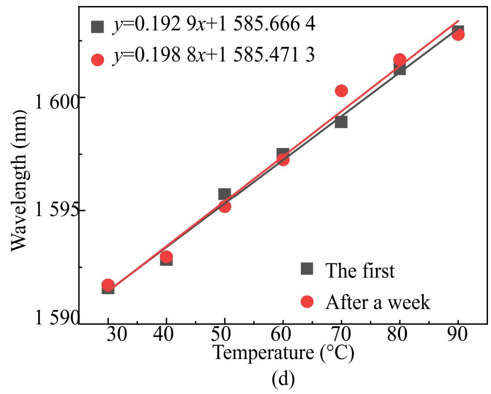

Fig.7 Comparison of repeated experiment results: (a) Dip 1; (b) Dip 2; (c) Dip 3; (d) Dip 4

It can be seen from Fig.7 that the comparison results of two experiments have little difference, so the sensor has good stability. Three repetitive experiments are performed, and the results are shown in Fig.8.

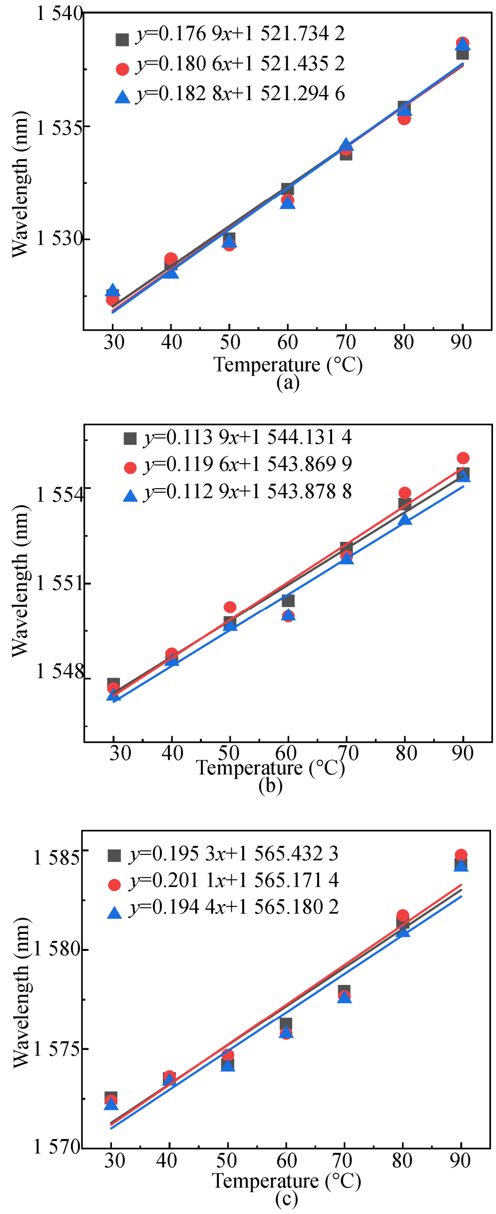

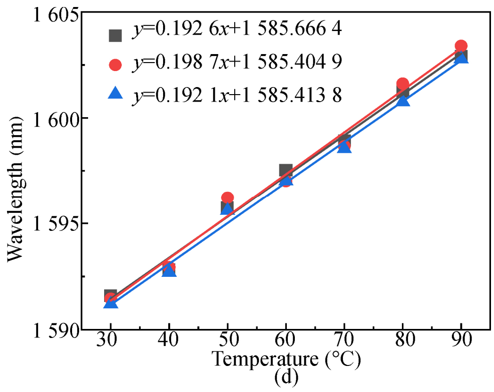

Fig.8 Repetitive experimental results: (a) Dip 1; (b) Dip 2; (c) Dip 3; (d) Dip 4

From Fig.8, it can be seen that the sensitivity and linearity of the sensor have not significantly changed, so the prepared sensor has good stability. The comparison between the sensitivity of the proposed sensor and other types of sensors is shown in Tab.3. We can see that the sensor presented in this paper has high temperature sensitivity.

Tab.3 Comparison of the performance for different sensors

Sensor	Temperature sensitivity (pm/°C)	Range (°C)
Ref.[12]	34.82	22—85
Ref.[13]	80.2	20—80
Ref.[14]	116	20—140
Ref.[15]	19.457	0—60
This paper	195.3	30—90

This paper mainly studies the temperature sensing characteristics of the LC coated GMF temperature sensor based on waist-enlarged taper. In the range of 30—90 °C, the temperature sensing characteristics of the sensor are studied. When the length of GMF is 2.5 cm, the temperature sensitivity can reach up to 195.3 pm/°C. The sensor can be used in biochemical, industrial production and other temperature detection areas.

Ethics declarations

Conflicts of interest

The authors declare no conflict of interest.

References

[1] GUO J Q, ZHOU M, LU Y L, et al. A temperature-insensitive polarization filter and a neotype sensor based on a hybrid-circular-hole microstructured optical fiber[J]. Optoelectronics letters, 2018, 14(4): 280-285.

[2] MCCARY K M, WILSON B A, BIRRI A, et al. Response of distributed fiber optic temperature sensors to high-temperature step transients[J]. IEEE sensors journal, 2018, 18(21): 8755-8761.

[3] LIU S H, ZHANG H L, LI T L, et al. Liquid core fiber interferometer for simultaneous measurement of refractive index and temperature[J]. IEEE photonics technology letters, 2019, 31(2): 189-192.

[4] LIN Q J, ZHAO N, YAO K, et al. Ordinary optical fiber sensor for ultra-high temperature measurement based on infrared radiation[J]. Sensors, 2018, 18(11): 4071.

[5] MORAIS J R W F, GIRALDI M T M R. Comparative performance analysis of relative humidity sensor based on intermodal interference using tapered square no-core optical fiber and tapered cylindrical optical fiber[J]. Optical and quantum electronics, 2019, 51(9): 288.

[6] WANG S Y, MA Y W, LI X A, et al. Highly sensitive torsion sensor based on triangular-prism-shaped long-period fiber gratings[J]. Chinese optics letters, 2021, 19(4): 041202.

[7] LV L, REN G J, LIU B, et al. Temperature influence on propagation characteristics of liquid crystal photonic crystal fiber of terahertz wave[J]. Journal of optoelectronics and advanced materials, 2011, 13(7): 755-759.

[8] HUANG Y J, WANG Y, MAO C, et al. Liquid-crystal-filled side-hole fiber for high-sensitivity temperature and electric filed measurement[J]. Micromachines, 2019, 10(11): 761.

[9] HU J Y, ZHOU D, SU Y M, et al. Fiber micro-tip temperature sensor based on cholesteric liquid crystal[J]. Optics letters, 2020, 45(18): 5209-5212.

[10] LIN W H, ZHOU S J, LIU Y B, et al. Liquid crystal-embedded hollow core fiber temperature sensor in fiber ring laser[J]. Applied sciences, 2021, 11(15): 7103.

[11] FU X H, LI D S, ZHANG Y X, et al. High sensitivity refractive index sensor based on cascaded core-offset splicing NCF-HCF-NCF structure[J]. Optical fiber technology, 2022, 68: 102791.

[12] OLIVEIRA R, OSORIO J H, ARISTIDES S, et al. Simultaneous measurement of strain, temperature and refractive index based on multimode interference, fiber tapering and fiber Bragg gratings[J]. Measurement science and technology, 2016, 27(7): 075107.

[13] LIU H, TAN C, ZHU C H, et al. Multi-parameters measurement based on cascaded Bragg gratings in magnetic fluid-infiltrated photonic crystal fibre[J]. Journal of modern optics, 2017, 64(8): 887-894.

[14] CAO X B, TIAN D D, LIU Y Q, et al. Sensing characteristics of helical long-period gratings written in the double-clad fiber by CO_2 laser[J]. IEEE sensor journal, 2018, 18(8): 7481-7485.

[15] LI C, NING T G, LI J, et al. Simultaneous measurement of refractive index, strain, and temperature based on a four-core fiber combined with a fiber Bragg grating[J]. Optics & laser technology, 2017, 90: 179-184.